Available online at www.sciencedirect.com

SciVerse ScienceDirect

Ceramics International 39 (2013) 7993–7999

CERAMICS INTERNATIONAL

www.elsevier.com/locate/ceramint

The evolution behavior of microstructures and optical properties of ZnO films using a Ti buffer layer

Xiaolei Zhang, Shuyi Ma*, Fuchao Yang, Qiang Zhao, Faming Li, Jing Liu

College of Physics and Electronic Engineering, Key Laboratory of Atomic and Molecular Physics & Functional Materials of Gansu Province, Northwest Normal University, Lanzhou, Gansu 730070, China

Received 30 October 2012; received in revised form 7 March 2013; accepted 16 March 2013
Available online 25 March 2013

Abstract

ZnO thin films without and with Ti buffer layer were prepared on Si and glass substrates by radio frequency (RF) magnetron sputtering. The effects of Ti buffer layer with different sputtering time on the microstructure and optical properties of ZnO thin films had been investigated by means of X-ray diffraction (XRD), energy dispersive spectrometer, X-fluorescence spectrophotometer and ultraviolet–visible spectrophotometer. The XRD results showed that the full-width at half-maximum (FWHM) for the ZnO (002) diffraction peak gradually decreased with the increase of sputtering time of Ti buffer layer, indicating that the crystalline quality of ZnO thin films was improved. The UV peak located at 390 nm, two blue peaks located at about 435 and 487 nm, two green peaks located at about 525 and 560 nm were observed from PL spectra. The PL spectra showed that the strongest blue light emission of ZnO films was obtained from Ti buffer layer with the sputtering time of 10 min. Meanwhile, the origins of the emission peaks were discussed through the Gaussian deconvolution. We also studied the optical band gaps.

Keywords: ZnO thin film; Ti buffer layer; RF magnetron sputtering; Photoluminescence

1. Introduction

Nanostructure materials have attracted the attention of researchers because of their tremendous technological importance. ZnO has emerged as one of the most promising nanostructure materials due to its optical and electrical properties, high chemical and mechanical stability, together with its abundance in nature, which makes it a lower cost material when compared to the most currently used transparent conductive oxide materials. ZnO has a wide band gap (3.37 eV) and a high exciton binding energy (~60 meV) [1], and it has been actively studied because of its potential application in both microelectronic and optoelectronic applications, such as solar cell windows [2], ultraviolet photo detectors [3], surface acoustic wave devices [4], gas sensors [5] and so on. ZnO films have been prepared through various approaches, i.e., pulsed laser deposition, metal–organic chemical vapor deposition, sol–gel and magnetron sputtering [6–9]. The most commonly used technique is the magnetron sputtering, because it is possible to obtain highly *c*-axis oriented and uniform films with excellent adhesion and packing density. A lot of research results show that the microstructure and optical properties of ZnO thin films have a direct connection with their crystalline qualities. Therefore, if one wants to obtain ZnO-based optoelectronic devices with good performance, one must begin with good quality ZnO thin films. But the quality of ZnO thin film is closely connected with the substrate materials. Up to now, ZnO films have been deposited on various substrates including sapphire [10], Si [1,6], $ScAlMgO_4$ [11], glass [7,8] and diamond [12], etc. Si is the most suitable substrate because of its low cost and additional advantages in integrated optoelectronic devices. However, ZnO films directly grown on Si substrates exhibit poor quality due to large mismatch of lattice constant and thermal expansion coefficients between ZnO and Si. Many different buffer layers such as Zn [13], ZnO [14,15], SiC [16], Ti [17] and TiO_2 [18] and so on, have been employed. In previous work, some groups have investigated the microstructure of ZnO nanorods on Ti-buffer layers [19] or ZnO films deposited on Ti buffer layers (ZnO/Ti) [17]. The choice of Ti as the initial buffer layer is based on the following consideration [17]: (1) Ti has the same hexagonal-close-packed (HCP) structure as ZnO. (2) The lattice mismatch between Ti and ZnO is 10% which is smaller than the lattice mismatch between Si and ZnO (15%), and

*Corresponding author. Tel.: +86 18919819403; fax: +86 9317971503.
E-mail address: xiaolei870421@163.com (S. Ma).

0272-8842/$ - see front matter
http://dx.doi.org/10.1016/j.ceramint.2013.03.066

thus it will reduce the effect of lattice mismatch. In this research, ZnO/Ti thin films were prepared on Si (100) and glass (Corning 7105) substrates by RF reactive magnetron sputtering. We conduct an investigation into the effects of Ti buffer on the structural, optical and photoluminescence properties of ZnO films. Furthermore, in order to explain the experimental results of photoluminescence, multi-peaks Gaussian fitting has been done to analyze the possible mechanism.

2. Experiments

ZnO and ZnO/Ti films were deposited on Si and glass substrates using the RF reactive magnetron sputtering technique. A high-purity Zn and Ti target (99.9999% purity, 60 mm in diameter), p-Si (100) and glass (Corning 7105) substrates were used in the experiments. The distance between target and substrate was fixed 50 mm. Before putting into the deposition chamber, Si substrates were dipped into the diluted HF solution (20%) to remove a native oxide layer on them, and then glass substrates and Si substrates were ultrasonically cleaned with acetone and alcohol in sequence for 15 min, and finally rinsed with distilled water and dried in nitrogen. The first step was that Ti thin films were deposited on substrates using RF reactive magnetron sputtering. The sputtering condition was as follows: the reactive pressure was 1 Pa; the RF power was 100 W; the flow rate of Ar gas was 20 sccm. After 0, 5, 10 and 15 min, Ti films with different thicknesses were obtained. The second step was that ZnO thin films were deposited on Ti buffer layer (ZnO/Ti) by sputtering Zn target using the RF reactive magnetron sputtering system. High purity Ar and O_2 were used as the sputtering and reactive gas, respectively. The deposition chamber was initially evacuated down to a residual pressure of 2×10^{-4} Pa. The Zn target was pre-sputtered for 10 min to remove surface contamination and maintain system stability. During deposition, the reactant pressure was maintained at 1 Pa, RF power was 100 W (716 V, 140 mA) and the substrate temperature was 500 °C. The sputtering time was 60 min. The annealing time was kept at the same value of 1 h in vacuum. ZnO film without and with Ti buffer layer which was deposited under the sputtering time of 0, 5, 10 and 15 min were labeled as samples a, b, c and d, respectively.

The film crystalline was characterized by using X-ray diffraction (XRD, D/Max-2400) with the Cu Kα radiation with $\lambda = 0.15406$ nm. The chemical components of the ZnO films with Ti buffer layer of different sputtering time were determined by energy dispersive spectrometer (EDS, S-4800). The absorption spectra were measured by using Lambda35UV/VIS. The photoluminescence (PL) spectra of the ZnO films measurements were carried out by using the excitation of Xe Lamp (RF-5301, wavelength 325 nm), and all spectra were taken at room temperature in air.

3. Results and discussion

3.1. Microstructure analysis

Fig. 1 shows XRD patterns of ZnO films with Ti buffer layer of different sputtering time grown on Si substrates: (a) 0 min, (b) 5 min, (c) 10 min, and (d) 15 min. The major peaks were observed at $2\theta = 31.8°$, 34.4°, 36.3° and 56.6°, which corresponded to the (100), (002), (101) and (110) plane reflections of a hexagonal ZnO (JCPDS 00-036-1451), demonstrating that the samples possess a polycrystalline hexagonal wurtzite structure. Ti phases which related to the buffer layers are not found in XRD patterns. This indicates that the Ti buffer layers have not changed the growth orientation of ZnO films and the ZnO films have a good *c*-axis orientation. The *c*-axis orientation in ZnO films can be understood by the "survival of the fastest" model proposed by Van der Drift [20]. According to this model, nucleation with various orientations can be formed at the initial stage of the deposition and each nucleus competes to grow but only nuclei having the fastest growth rate can survive, i.e. *c*-axis orientation is achieved.

In Fig. 1, it can be seen that the intensity of (002) diffraction peak increases after Ti buffer layer is introduced (sample b). However, the diffraction intensity gradually decreases as the sputtering time of Ti layers increases from 5 min to 15 min. Fig. 2 shows enlarged figure of (002) diffraction peak for ZnO films with Ti buffer layer of different sputtering time. The results reveal that the diffraction angle of ZnO/Ti(002) diffraction peaks shifted to lower angle compared with the standard XRD spectrum of ZnO power (34.43°), implying that the lattice constant *c* changed for all ZnO/Ti films. These changes were mainly caused by the strain of ZnO/Ti films.

To obtain the film stress with a hexagonal crystal structure, the following formula is used [21]:

$$\sigma = \frac{2c_{13}^2 - c_{33}(c_{11} + c_{12})}{2c_{13}} \times \frac{c - c_0}{c_0} \quad (1)$$

The values of the elastic constant from single crystalline ZnO are employed, $c_{11} = 208.8$ GPa, $c_{33} = 213.8$ GPa, $c_{12} = 119.7$ GPa and $c_{13} = 104.2$ GPa. *c* is the lattice constant of ZnO film, and c_0 is the lattice constant of standard ZnO powder. The calculated results are shown in Table 1. All the samples have a negative stress, which indicates that the films are in compression condition. Namely, the stresses that exist in the films are compression stress. Basically the stress in film

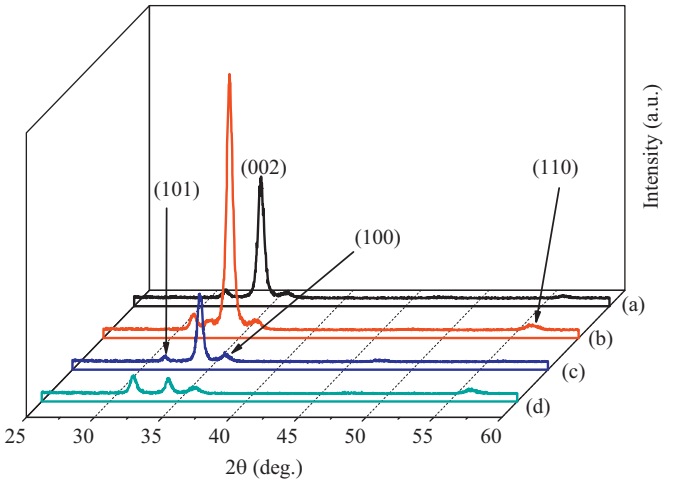

Fig. 1. XRD patterns of ZnO films with Ti buffer layer of different sputtering time grown on Si substrate: (a) 0 min, (b) 5 min, (c) 10 min, and (d) 15 min.

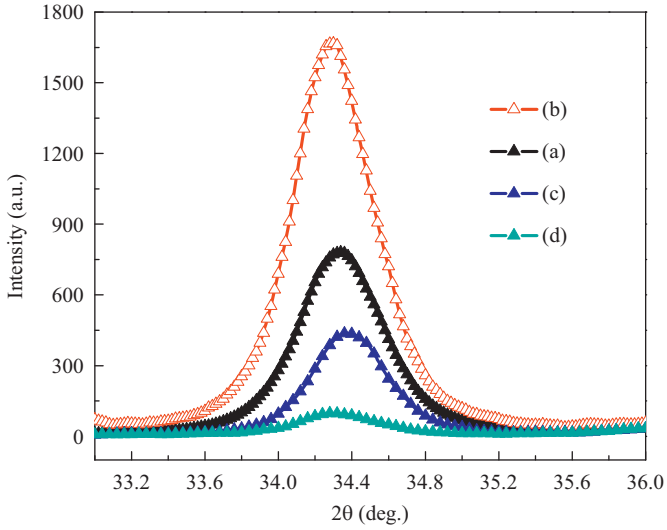

Fig. 2. Enlarged figure of (002) diffraction peak for ZnO films with Ti buffer layer of different sputtering time.

Table 1
Experimental results of ZnO thin films with Ti buffer at different sputtering time: (a) 0 min, (b) 5 min, (c) 10 min, and (d) 15 min.

Sample	FWHM (deg)	c (nm)	σ (GPa)	D (nm)	E_g (eV)	E_0 (eV)
a	0.494	0.5218	−0.5370	16.6	3.225	0.0769
b	0.474	0.5226	−0.8951	17.3	3.197	0.0773
c	0.439	0.5216	−0.4476	18.7	3.205	0.0816
d	0.424	0.5226	−0.8951	19.3	3.217	0.0749

includes a thermal stress originating from thermal mismatch between film and substrate and another intrinsic stress originating from the crystal defects of thin film [22]. Since all ZnO thin films were prepared with same condition, intrinsic stress originating from the crystal defects of thin film must have almost same value for all ZnO thin films. So these stresses are mainly caused by the thermal stress originating from lattice mismatch between films and substrates.

The crystalline plane distance is calculated based on the X-ray diffraction theory [23]:

$$\lambda = 2dsin\,\theta \tag{2}$$

where λ is the X-ray wavelength (0.15406 nm), θ is the diffraction angle and d denotes the crystalline plane distance of indices (h, k, l), which are the Miller indices. Considering the interplanar space for the hexagonal system [24];

$$\frac{1}{d} = \left(\frac{4}{3}\frac{h^2 + hk + k^2}{d^2} + \frac{l^2}{c^2}\right)^{-1/2} \tag{3}$$

We calculated the unit cell parameters of the ZnO films. As shown in Table 1, it is found that the crystal lattice constant c is 0.5218, 0.5226, 0.5216 and 0.5226 nm. As we know, the crystal lattice constant c_0 for powder ZnO crystal is 0.5206 nm. As a result, the crystal lattice constant of all samples are larger than that of standard ZnO powder.

The average crystallite size in the films can be calculated using the Scherrer formula, using FWHM values of the XRD diffraction peaks as follows [15]:

$$D = \frac{0.9\lambda}{\beta cos}\,\theta \tag{4}$$

where β denotes FWHM and θ is the Bragg angle of the (002) diffraction peak. Table 1 shows the calculation results. It can be seen that the values of the crystallite size for the films are on the order of nanometers (16.6–19.3 nm) and the crystallite size for ZnO/Ti films are larger than ZnO/Si film. With the increase of the sputtering time of Ti buffer, we gradually observe a decrease in the FWHM of XRD for ZnO films. The FWHM of XRD links the crystallite size. The decrease of FWHM value reveals that Ti buffer enhances the crystal quality of ZnO film. However, the intensity of (002) diffraction peak decreases and the intensity of (100) diffraction peak increases when the sputtering time of Ti buffer increase up to 15 min. Based on the above analysis, we believe that the sputtering time of Ti buffer is 10 min for the better growth of ZnO films.

3.2. Element composition analysis

For the as-grown ZnO films deposited by the physical deposition method such as pulsed laser deposition, magnetron sputtering, and electron beam evaporation and so on, the chemical components (Zn and O) are nonstoichiometric [18]. Fig. 3 shows the EDS spectra of (a) ZnO/Si and (b) ZnO/Ti/Si with the sputtering time of Ti buffer layer at 10 min. The peaks in the spectrum agreed to O, Si (come from the silicon substrate) and Zn signals. The results reveal that the stoichiometry in ZnO films grown by RF magnetron sputtering is far smaller than one and there were too many Zn atoms, thus resulting in the generation of many oxygen vacancies during deposition. Therefore, many lattice defects and surface defects are contained in the as-grown ZnO films.

3.3. Absorption and optical band analysis

As a directed band gap semiconductor, the band of ZnO film is an important parameter. The optical band gap was determined from the absorption spectra using the Tauc relationship as follows [25]:

$$\alpha h\nu = A(h\nu - E_g)^n$$

where α is the absorption coefficient, A is a constant, h is the Planck constant, ν is the photon frequency, E_g is the optical band gap, and n is the 1/2 for direct band gap semiconductors.

The E_g value can be determined by extrapolating the linear absorption edge part of the curves toward the $h\nu$ axis. The photon energy at the point where $(\alpha h\nu)^2$ is zero is E_g. Fig. 4 shows the plot of $(\alpha h\nu)^2$ versus $h\nu$ of ZnO films without and with Ti buffer layers at different sputtering time according to the absorption spectra measured (here is not shown). As can be seen from Table 1, the optical band gap values for the samples are 3.225, 3.197, 3.205 and 3.217 eV at the wavelength 384, 388, 387 and 385 nm, respectively. We can see that the E_g of

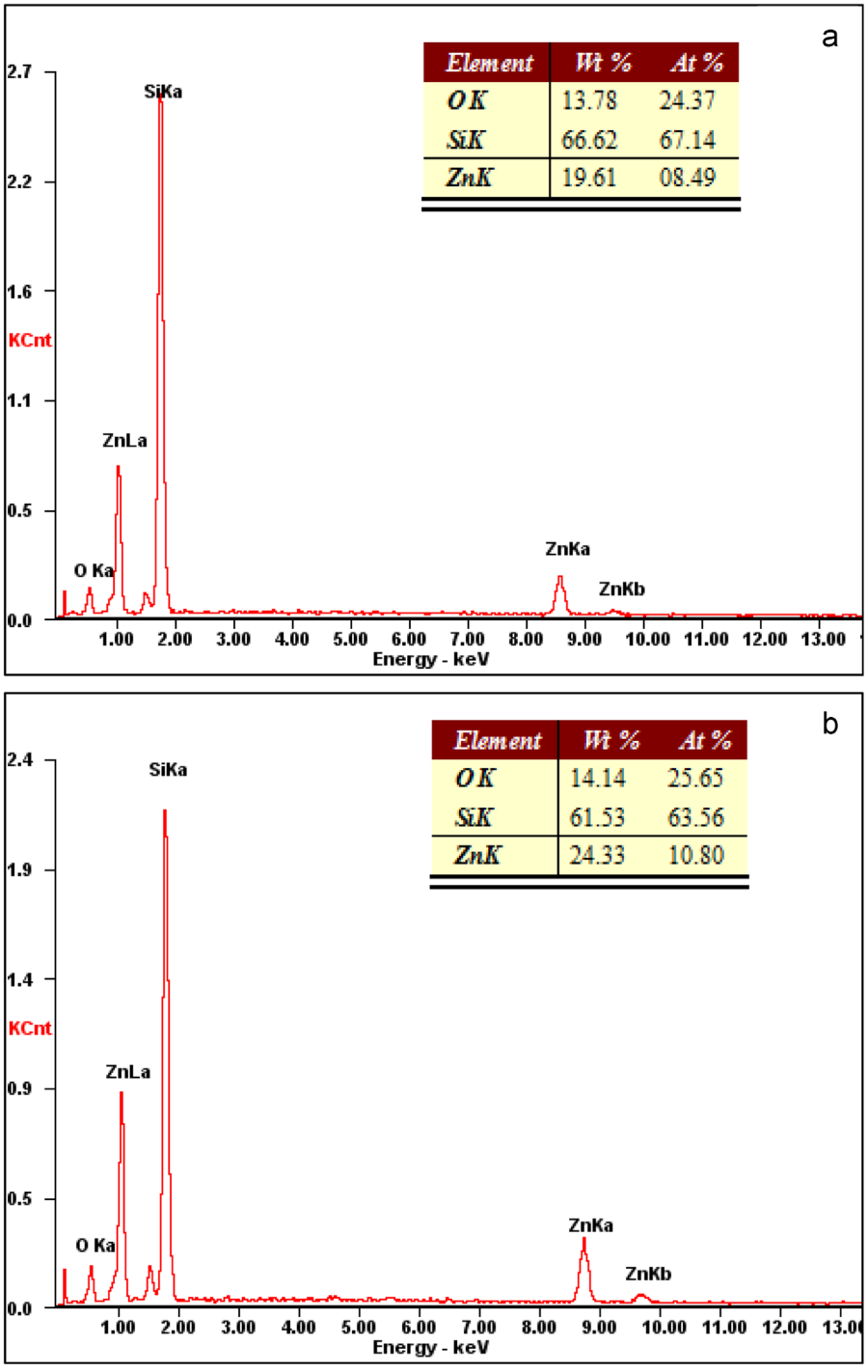

Fig. 3. The EDS spectra of (a) ZnO/Si film and (b) ZnO/Ti/Si film with the sputtering time of Ti buffer layer at 10 min.

ZnO thin films with Ti buffer red shift compared with ZnO thin films without buffer. Marotti et al. [26] have reported that the band gap and the absorption edge of nanostructure materials shifted due to quantum size effects (QSE), resulting from the changing of crystallite size. In their views, the band gap of our samples should be gradually decreased. However, the variation of band gap and crystallite size is not accordant in our paper. Peng et al. [27] have reported that the inner strain will be responsible for the changes of the band gaps. This is because the compressed lattice will provide a wider band gap because of the increased repulsion between the oxygen 2p and the zinc 4s bands [27]. So we attributed the shift of band gap to both crystallite size and the strain.

When the photon energy ($h\nu$) is near the E_g and less than E_g, the absorption coefficient (α) follows the experimental law [28]:

$$\alpha = \alpha_0 exp\left(\frac{h\nu}{E_0}\right)$$

where α_0 is a constant and E_0 is an experimental parameter that can be used to characterize the effects of all possible defects in

films. We can see that there is a linear relationship to ln α and the photon energy ($h\nu$). E_0 can be obtained from the slope.

The $ln[(h\nu)]$ versus photon energy plots for the ZnO thin films without and with Ti buffer layers at different sputtering time are shown in Fig. 5. The inset of Fig. 5 shows the partial enlarged figure of Fig. 5 ranging from 3.11 to 3.29 eV. E_0 was calculated from the reciprocal gradient of the linear portion of these curves and is shown in Table 1.

As can be seen from Table 1, E_0 are 0.0769, 0.0773, 0.0816 and 0.0749 eV. Changes of the E_0 are consistent with the defect density in the film. In our study, E_0 increases after Ti buffer was introduced, indicating defect density in the film increases. With the increase of sputtering time for Ti buffer, E_0 gradually increases, indicating defect density in the film increases. As the sputtering time of Ti buffer is15 min, E_0 decreases, indicating defect density in the film decreases. This result was in good agreement with analysis of PL.

3.4. Photoluminescence analysis

PL spectrum is a powerful tool to characterize the optical quality of semiconductor materials, such as PL peak intensity correlating directly with the defects densities in materials. Fig. 6 depicts the room PL spectra and multi-peak Gaussian fitting spectra for ZnO thin films with Ti buffer layer of different sputtering time: (a) 0 min, (b) 5 min, (c) 10 min, and (d) 15 min. Generally speaking, the PL spectrum of ZnO film consists of the UV band and the visible emission broadband. The UV emission is ascribed to the near band edge emission from the recombination of excitons [29]. It is widely accepted that the visible emission is mainly due to the structural defects which are related to deep-level emissions (DLE), such as zinc interstitials, zinc vacancies, oxygen interstitials, oxygen vacancies and so on [30].

From Fig. 6, one sees that the UV emission located at about 390 nm, two blue peaks located at about 442 and 487 nm and

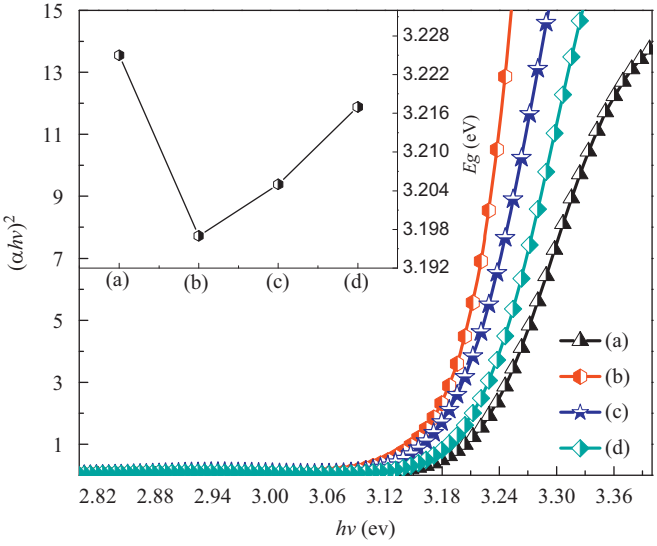

Fig. 4. Plot of $(\alpha h\nu)^2$ versus $h\nu$ of ZnO films without and with Ti buffer layer at different sputtering time.

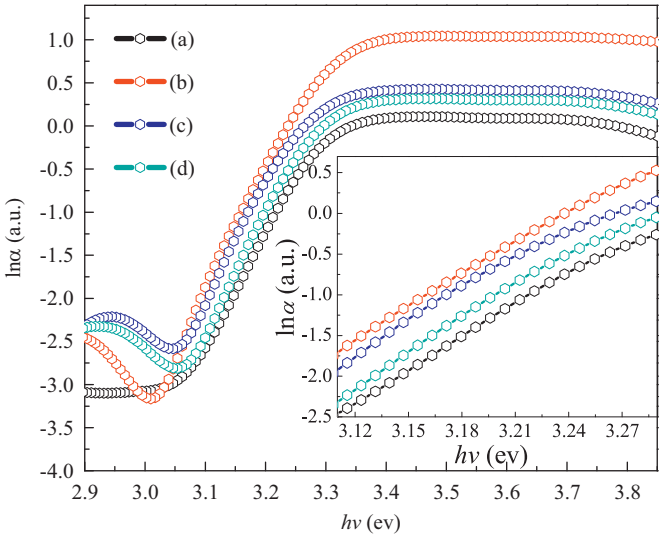

Fig. 5. ln α of ZnO thin films without and with Ti buffer layer at different sputtering time as a function of $h\nu$. The inset shows the enlarged Fig. 4 ranging from 3.11 to 3.29 eV. (For interpretation of the references to color in this figure legend, the reader is referred to the web version of this article.)

two green peaks located at about 525 and 560 nm were observed from the PL spectra when ZnO film was prepared on Si substrate. As a Ti buffer layer was introduced, there occurred no other new emission peak in ZnO/Ti films while the intensity of above emission peaks increased. In addition, the emission center of 442 nm shifted to 435 nm. Zhang et al. [16] believe the shift of deep level emissions from ZnO films on Si and SiC buffer layer may be attributed to the different defect centers associated to the stress, strain and dislocation in samples. It was evident that PL emission characteristic of ZnO films are strongly dependent on the crystal quality of films. As the sputtering time of Ti buffer was increased from 5 min to 15 min, the intensities of five peaks increased a maximum at the sputtering time of 15 min of Ti buffer and then decreased. This PL behavior means that the crystal quality of ZnO films is greatly dependent on the sputtering time of Ti buffer. The same trend was also observed in GaN films grown on ZnO buffer layers [31] and ZnO films grown on ZnO buffer layers [15].

In Fig. 6, we could observe the UV emission located at 390 nm. It is generally considered it results from recombination of free exaction and its intensity is related to both the stoichiometry and the crystalline quality of ZnO film.

The origins of deep-level emissions PL had been investigated for a long time. The as-grown ZnO thin film is an n-type semiconductor and it means that Zn interstitials and oxygen vacancies are main donor defects while Zn vacancies and oxygen interstitials are main acceptor defects in intrinsic ZnO [32]. Kohan et al. [33] have calculated the energy levels of defects in ZnO films by the full-potential linear muffin-tin orbit method. According to the calculated results of them, the energy interval between the donor level formed by Zn interstitials defects and the top of the valence band was about 2.87 eV and the energy interval between the shallow donor level formed by Zn interstitials to shallow acceptor level formed by Zn vacancies was about 2.57 eV, which were well

consistent with the energies of the two blue peaks at 435 nm (2.86 eV) and 487 nm (2.55 eV) in our experiment. Therefore, the two blue emission peaks were assigned to the electron transition from Zn interstitials levels to the top of valence band and the energy levels of Zn interstitials to Zn vacancies, respectively.

In Fig. 6, a green peak located at about 525 nm (2.37 eV) was observed. It is a relatively common phenomenon, but its emission mechanism remains controversial. There are three main viewpoints as follows [18]: (1) the green emission results from oxygen vacancies in ZnO thin films, (2) the green emission to oxygen interstitials and (3) the green emission corresponds to the local level composed by oxide antisite defect rather than oxygen vacancy or oxygen interstitial. In our experiments, ZnO thin films were performed in an oxygen poor environment. Some oxygen vacancies might appear in the deposited films. And from Fig. 3, we can find that the chemical components (Zn and O) in ZnO and ZnO/Ti thin film are nonstoichiometric. Many lattice defects are contained in the as-grown ZnO films and most lattice defects are interstitial Zn and oxygen vacancies. Vanheusden et al. [30] reported that the energy interval between the top of valance band and the deep oxygen vacancy level is about 2.4 eV. Kang et al. [34] concluded that the mechanism of green peak located at 530 nm in ZnO was the electron transition from deep donor level formed by the oxygen vacancies to valence band level. The green peak (525 nm, 2.37 eV) observed in this work was fully supported by Vanheusden and Kang's results. So, the green peak located at 525 nm (2.37 eV) may correspond to the electron transition from deep oxygen vacancy level to the top of valance band. A weak and broad green peak occurred at about 560 nm (2.22 eV) was also observed in PL. This peak was rarely reported in the literature. Therefore, we believe the origin of the green peak (560 nm) was attributed to oxygen interstitials and oxygen vacancies [35].

4. Conclusion

In summary, Ti buffer layers with different sputtering time (0, 5, 10 and 15 min) were first deposited on Si substrates using the RF magnetron sputtering system, and then ZnO thin films were deposited on Ti buffer layers by the RF magnetron sputtering system. Effects of buffer layers on ZnO films were studied. XRD measurements reveal that the FWHM for the ZnO (002) diffraction peak gradually decreases with the increase of sputtering time of Ti buffer layer. Considering the FWHM of (002), the grain size, the stress, the intensity of (002) diffraction peak and the intensity of luminescence peak, the sputtering time of Ti buffer is 10 min for the better growth of ZnO films. Three main emission peaks including the UV emission located at 390 nm, two blue peaks located at about 435 nm and 487 nm and two green peaks located at about 525 nm and 560 nm were observed from PL spectra. The UV emission may originate from recombination of free exaction. Two blue emission peaks were assigned to the electron transition from the Zn interstitials levels to the top of valence

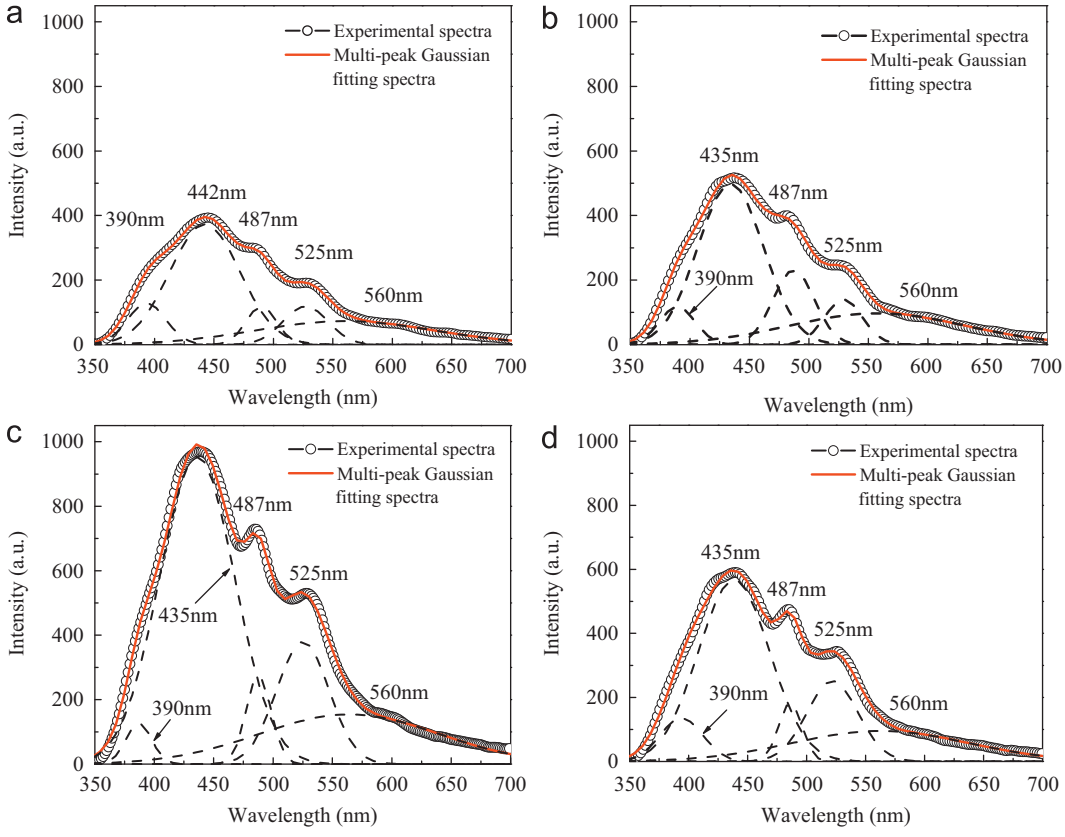

Fig. 6. The room temperature PL spectra of ZnO films with Ti buffer layer of different sputtering time grown on Si substrates: (a) 0 min, (b) 5 min, (c) 10 min, and (d) 15 min.

band and the energy levels of Zn interstitials to Zn vacancies. The green peak located at 525 nm may correspond to the electron transition from deep oxygen vacancies level to the top of valance band and the green peak located at 560 nm was attributed to oxygen interstitials and oxygen vacancies.

Acknowledgments

The work is sponsored by the National Natural Science Foundations of China (Grant no. 10874140), the College Basic Scientific Research Operation Cost of Gansu Province (2010–2012) and the Scientific Research Foundation for the Returned Overseas Chinese Scholars, State Education Ministry. We are also grateful to David Kennedy (from the USA) for checking English.

References

[1] Y.G. Wang, S.P. Lau, H.W. Lee, S.F. Yu, B.K. Tay, X.H. Zhang, H.H. Hng, Photoluminescence study of ZnO films prepared by thermal oxidation of Zn metallic films in air, Journal of Applied Physics 94 (2003) 354–358.

[2] W.J. Jeong, S.K. Kim, G.C. Park, Preparation and characteristic of ZnO thin film with high and low resistivity for an application of solar cell, Thin Solid Films 506–507 (2006) 180–183.

[3] H.S. Bae, Seongil Im, Ultraviolet detecting properties of ZnO-based thin film transistors, Thin Solid Films 469–470 (2004) 75–79.

[4] W. Shih, M. Wang, I. Nan Lin, Characteristics of ZnO thin film surface acoustic wave devices fabricated using nanocrystalline diamond film on silicon substrates, Diamond and Related Materials 17 (2008) 390–395.

[5] H. Xu, X. Liu, D. Cui, M. Li, M. Jiang, A novel method for improving the performance of ZnO gas sensors, Sensors and Actuators B 114 (2006) 301–307.

[6] J. Zhao, L. Hu, W. Wang, W. Liu, A. Gong, Effects of growth atmosphere and homo-buffer layer on properties of ZnO films prepared on Si(111) by PLD, Vacuum 82 (2008) 664–667.

[7] X.L. Chen, X.H. Geng, J.M. Xue, D.K. Zhang, G.F. Hou, Y. Zhao, Temperature-dependent growth of zinc oxide thin films grown by metal organic chemical vapor deposition, Journal of Crystal Growth 296 (2006) 43–50.

[8] R. Navamathavan, C.K. Choi, E. Yang, J. Lim, D. Hwang, S. Park, Fabrication and characterizations of ZnO thin film transistors prepared by using radio frequency magnetron sputtering, Solid-State Electronics 52 (2008) 813–816.

[9] J. Sengupta, R.K. Sahoo, K.K. Bardhan, C.D. Mukherjee, Influence of annealing temperature on the structural, topographical and optical properties of sol–gel derived ZnO thin films, Materials Letters 65 (2011) 2572–2574.

[10] J. Lim, K. Shin, H.W. Kim, C. Lee, Effect of annealing on the photoluminescence characteristics of ZnO thin films grown on the sapphire substrate by atomic layer epitaxy, Materials Science and Engineering: B 107 (2004) 301–304.

[11] B. Wessler, A. Steinecker, W. Mader, Epitaxial growth of ZnO thin films on $ScAlMgO_4$ (0001) by chemical solution deposition, Journal of Crystal Growth 242 (2002) 283–292.

[12] J.J. Chen, F. Zeng, D.M. Li, J.B. Niu, F. Pan, Deposition of high-quality zinc oxide thin films on diamond substrates for high-frequency surface acoustic wave filter applications, Thin Solid Films 485 (2005) 257–261.

[13] C. Lee, A. Park, Y.J. Cho, W.I. Lee, H.W. Kim, The role of the Zn buffer layers in the structural and photoluminescence properties of ZnO films on Zn buffer layers deposited by RF magnetron sputtering, Vacuum 82 (2008) 1364–1366.

[14] D.J. Park, J.Y. Lee, T.E. Park, Y.Y. Kim, H.K. Cho, Improved microstructural properties of a ZnO thin film using a buffer layer in-situ annealed in argon ambient, Thin Solid Films 515 (2007) 6721–6725.

[15] R. Hong, J. Shao, H. He, Z. Fan, Influence of buffer layer thickness on the structure and optical properties of ZnO thin films, Applied Surface Science 252 (2006) 2888–2893.

[16] Y. Zhang, H. Zheng, J. Su, B. Lin, Z. Fu, Effects of SiC buffer layer on the optical properties of ZnO films grown on Si(111) substrates, Journal of Luminescence 124 (2007) 252–256.

[17] F. Li, D. Li, J. Dai, H. Su, L. Wang, Y. Pu, W. Fang, F. Jiang, Effect of the initial thin Ti buffer layers on the quality of ZnO thin films grown on Si(111) substrates by MOCVD, Superlattices and Microstructures 40 (2006) 56–63.

[18] L. Xu, L. Shi, X. Li, Effect of TiO_2 buffer layer on the structural and optical properties of ZnO thin films deposited by E-beam evaporation and sol–gel method, Applied Surface Science 255 (2008) 3230–3234.

[19] C.H. Kwak, B.H. Kim, C.I. Park, S.Y. Seo, S.H. Kim, S.W. Han, Synthesis and microstructural properties of ZnO nanorods on Ti-buffer layers, Journal of Crystal Growth 314 (2011) 264–267.

[20] A. Van der Drift, Evolutionary selection: a principle governing growth orientation in vapour-deposited layers, Philips Research Report 22 (1967) 267–288.

[21] Y.M. Tao, S.Y. Ma, H.X. Chen, J.X. Meng, L.L. Hou, Y.F. Jia, X.R. Shang, Effect of the oxygen partial pressure on the microstructure and optical properties of ZnO:Cu films, Vacuum 85 (2011) 744–748.

[22] C. Wang, Z. Chen, H. Hu, D. Zhang, Effect of the oxygen pressure on the microstructure and optical properties of ZnO films prepared by laser molecular beam epitaxy, Physica B 404 (2009) 4075–4082.

[23] W. Zhang, J. Zhao, Z. Liu, Z. Liu, Z. Fu, Influence of growth temperature of TiO_2 buffer on structure and PL properties of ZnO films, Applied Surface Science 256 (2010) 4423–4425.

[24] L. Ma, X. Ai, X. Huang, S. Ma, Effects of the substrate and oxygen partial pressure on the microstructures and optical properties of Ti-doped ZnO thin films, Superlattices and Microstructers 50 (2011) 703–712.

[25] M. Girtan, G. Folcher, Structural and optical properties of indium oxide thin films prepared by an ultrasonic spray CVD process, Surface and Coatings Technology 172 (2003) 242–250.

[26] R.E. Marotti, P. Giorgi, G. Machado, E.A. Dalchiele, Crystallite size dependence of band gap energy for electrodeposited ZnO grown at different temperatures, Solar Energy Materials and Solar Cells 90 (2006) 2356–2361.

[27] L.P. Peng, L. Fang, W.D. Wu, X.M. Wang, Y.Y. Wang, The structure and optical properties of ZnO films on various $LiNbO_3$ substrates, Vacuums 86 (2012) 1147–1149.

[28] F. Urbach, The long-wavelength edge of photographic sensitivity and of the electronic absorption of solids, Physical Review 92 (1953) 1324-1324.

[29] S. Wang, G. Xia, J. Shao, Z. Fan, Structure and UV emission of nanocrystal ZnO films by thermal oxidation of ZnS films, Journal of Alloys Compounds 424 (2006) 304–306.

[30] K. Vanheusden, C.H. Seager, W.L. Warren, D.R. Tallant, J.A. Voigt, Correlation between photoluminescence and oxygen vacancies in ZnO phosphors, Applied Physics Letters 68 (1996) 403–406.

[31] S. Xue, X. Zhang, R. Huang, H. Zhuang, Effects of the sputtering time of ZnO buffer layer on the quality of GaN thin films, Applied Surface Science 254 (2008) 6766–6769.

[32] J.J. Ding, S.Y. Ma, H.X. Chen, X.F. Shi, T.T. Zhou, L.M. Mao, Influence of Al-doping on the structure and optical properties of ZnO films, Physica B 404 (2009) 2439–2443.

[33] A.F. Kohan, G. Ceder, D. Morgan, Chris G. Van de Walle, First-principles study of native point defects in ZnO, Physical Review B: Condensed Matter 61 (2000) 15019–15027.

[34] J.S. Kang, H.S. Kang, S.S. Pang, E.S. Shim, S.Y. Lee, Investigation on the origin of green luminescence from laser-ablated ZnO thin film, Thin Solid Films 443 (2003) 5–8.

[35] V.S. Khomchenko, T.G. Kryshtab, A.K. Savin, L.V. Zavyalova, N.N. Roshchina, V.E. Rodionov, O.S. Lytvyn, V.I. Kushnirenko, V.B. Khachatryan, J.A. Andraca-Adame, Fabrication and properties of ZnO:Cu and ZnO:Ag thin films, Superlattices and Microstructures 42 (2007) 94–98.